

Design and Fabrication of a 3D-Printed Axial Flux 3-Phase Permanent Magnet Motor for Drone Applications

Steven A. Abrego*, Anchit Narain*

*Department of Electrical Engineering, Stanford University, Stanford, CA, 94305

Abstract—This paper discusses the design and fabrication of a single stator, dual rotor axial flux 3-phase permanent magnet motor for drone applications. The motor is composed of 3D printed parts, and is driven using an electronic speed controller and a servo tester. Various motor constants were calculated for this motor as well as lift generated (when attached to a propeller) as a function of RPM. This motor has a Kv rating of 5080 and is capable of 5,000+ RPM at 10V.

Index Terms—Axial flux, permanent magnet motor, back EMF, motor constants, drone application, 3D print

I. INTRODUCTION

There has been a growing interest in axial flux permanent magnet (AFPM) motors for automotive, aeronautic, and unmanned aerial vehicle (UAV) applications due to their higher torque density compared to other electric motors [1]. AFPM motors can also be designed with several rotors and/or several stators to improve their torque-to-weight performance.

However, the difficulty in manufacturing iron components for AFPM geometries has limited the widespread adoption of these motors [2]. The recent development of iron-less AFPM motor designs (i.e. double sided AFPM motors with internal stators) have significantly reduced weight compared to iron AFPM designs without significant reduction in performance [1].

AFPM motors are ideal for UAV applications as they are more compact than radial flux motors, so their thrust-to-weight performance is better than that of radial flux motors [3]. Iron-less AFPM motors are lightweight, have high efficiency, and have no cogging torque, so torque ripples are reduced, resulting in quieter flight [1].

For our final project in EE 157: Electric Motors for Renewable Energy, Robotics, and Electric Vehicles, we designed and fabricated a 3D printed 3-phase AFPM motor for drone applications. We calculated the motor constants K_b , K_τ , K_m of our designed motor before measuring the lift it generated as a function of RPM when attached to a drone propeller. We hope that characterizing our designed motor configuration will provide a baseline for others to understand and improve upon it for future UAV applications.

II. MOTOR DESIGN

We designed an iron-less AFPM motor with 8 pole pairs and 6 coils on each of the two faces of the stator, yielding a total of 12 coils embedded in the stator. To prevent the motor from stalling, there must be an imbalance in the number of pole pairs and number of coils per face. We used a single stator, dual rotor design (as seen in [1]) to direct the magnetic flux across the face of the stator. Using a dual rotor configuration

allows both rotors to rotate synchronously due to the magnetic attraction between opposite poles on different sides of the stator.

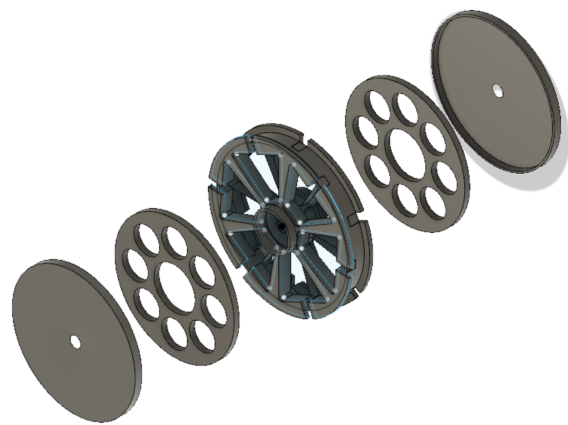


Fig. 1. Exploded view of Autodesk Fusion 360 motor configuration. The configuration consists of (2) rotors, (2) magnet holders, and (1) stator. The rotors (outer components), stator (middle component), and magnet holders will have a single shaft through all components. The stator has a ball bearing embedded within the center hole connecting to the shaft for decreased friction and as angular independence from the spinning magnet holder and rotor. The magnet holders embed into the rotor and spin synchronously.

We modeled the motor components in Autodesk Fusion 360, as shown in Fig. 1. The inner diameter of the stator was 19 mm to allow for the 19 mm outer diameter ball bearing and 6 mm shaft to fit within the stator. The outer diameter of the stator was 82.55 mm. The scale of the motor was chosen to allow for reasonably sized coil housing areas, since all coils were wound by hand. We used 15 mm diameter neodymium magnets and thus the designed magnet holders had a diameter of 70 mm to evenly space 8 neodymium magnets per magnet holder. The inner diameter of the rotor was also 70 mm to allow for the magnet holder to fit within the bore of the rotor.

We chose to house 6 coils on each of the two faces of the stator to allow for 12 total coils. This meant there were 4 coils for each of the three phases. The coils were connected in the configuration shown in Fig. 2 [4]. Note that Fig. 2 just shows the winding configuration for one of the three phases (A). The other two phases (B and C) were wired identically but are not shown in the diagram.

III. MOTOR FABRICATION

As mentioned before, one of the key factors limiting the widespread adoption of AFPM motors is how difficult it is

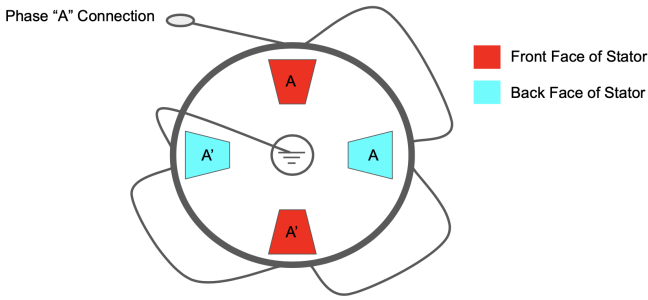


Fig. 2. Winding configuration for a single phase, A, of the motor. The front side of the stator (depicted in red) housed the windings denoted as A and A'. Similarly the back side of the stator (depicted in blue) mimics the front face but rotated 90° clockwise. This winding configuration must be consistent with the B and C phases (not shown). Each phase is offset 45° clockwise to allow for motor rotation.

to machine AFPM geometries. As such, we chose to 3D print our AFPM stator, rotors, and magnet holders to reduce time and cost of manufacturing. We 3D printed all the above components out of PLA using Prusa MK3S 3D printers. The print settings for all printed components was set to 0.15 mm quality (i.e. no printed component was finer than 0.15 mm in any dimension). The stator was printed at 15% infill density whereas the rotors and magnet holders were printed at 20% infill density. We chose these low infill densities to reduce print time and keep our printed components as light as possible for UAV applications.

#24 AWG wire was used to wind each of the coils, yielding 7 turns per coil. At 4 coils per phase, our design allocated 28 turns of wire for each of the three phases.

Fig. 3 shows all the 3D printed components used to fabricate our motor.

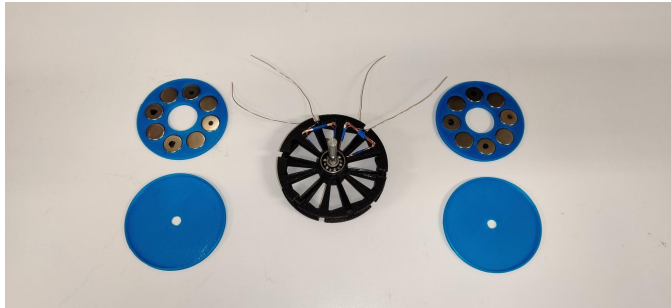


Fig. 3. Image of the 3D printed components used to fabricate our motor. The stator (black) has two coils (7 turns each) embedded into it, showing where the coils are housed and how their leads come out to be soldered to other coils. The magnet holders (blue, top right and left) are embedded into the rotors (blue, bottom right and left) and spin synchronously with the rotors. The ball bearings and motor shaft are also shown embedded in the middle of the stator, though these components were purchased, not 3D printed.

IV. SYSTEM DESIGN

We used an electronic speed controller (ESC) and a servo tester to drive our motor. We had some difficulty configuring

the ODrive v3.6 to drive our motor and as such resorted to the ESC setup. The ESC setup allowed us to coarsely vary the input voltage, thus varying the angular velocity of the motor. Once we were able to spin the motor, we were able to calculate its motor constants and characterize the motor and propeller system's generated lift as a function of RPM. All experiments were conducted in the EE157 lab in the basement of the Packard Building. A system diagram is outlined in Fig. 4.

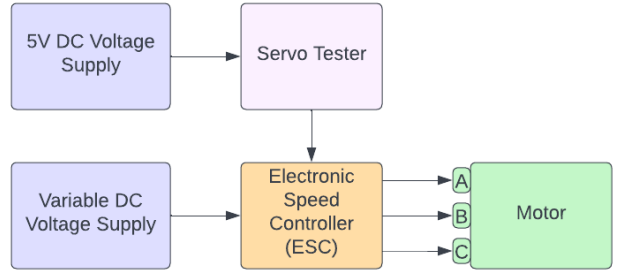


Fig. 4. System Diagram of configuration using an electronic speed controller and a servo tester. The "A, B, C" blocks connected to the motor denote the three phases of the motor. The variable DC voltage supply ranged from 0V-24V, and could supply up to 20 A. For the purposes of this final project, the variable DC voltage supply was fixed at 10V and modulated using the servo tester.

V. SYSTEM SETUP

After the motor was assembled, the following procedure was followed to set up the motor for testing:

- 1) Create motor housing (see Fig. 5). Attach the motor to the housing at the stator.
- 2) Connect (3) Differential probes to the oscilloscope, as well as across each of the three phases to the common ground (GND) lead.
- 3) Manually spin the motor and capture the motor's back EMF waveforms (see Fig. 6). If the three phases are wired correctly, the three waveforms should be 120° out of phase from one another.
- 4) Connect the three leads of the motor to the three leads of the electronic speed controller (ESC).
- 5) Connect the red and black leads of the ESC to the variable DC voltage supply.
- 6) Connect the black and white lead of the ESC to the servo tester.
- 7) Connect the other end of the servo tester to the 5V DC voltage supply.
- 8) Now connect (3) current probes across each of the three phases of the motor.
**Note: Calibrate current probes before taking measurements!
- 9) Power on both voltage supplies, setting the variable voltage supply to 10V.
- 10) The servo tester should begin beeping. Slowly turn its dial until the motor begins to oscillate. Manually

- kickstart the motor and it should begin spinning on its own.
- 11) Capture the waveforms while the motor is spinning on its own. The three waveforms should be 120° out of phase from one another. This is the current waveform (see Fig. 8).
 - 12) Attach the propeller to the shaft of the motor, ensuring that the propeller and the shaft spin synchronously.
 - 13) Place the housing and motor on a scale. Tare the scale. Drive the motor, ensuring that the motor is spinning such that the propeller is pushing the motor and housing down into the scale. Vary the speed of the motor. Measure the scale reading and capture the current waveform. Use these values to create thrust values as a function of RPM (see section VII for procedure).

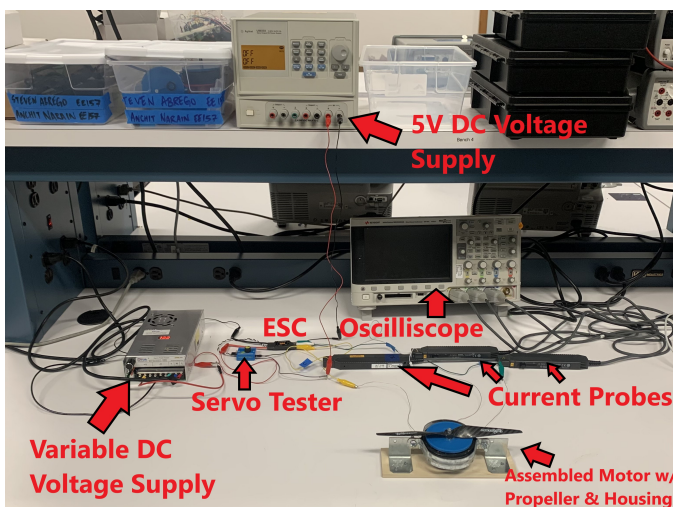


Fig. 5. Completed system setup with assembled motor and attached propeller along with housing to hold the motor. Current probes were used to capture the current waveforms shown in Fig. 8.

VI. MOTOR CHARACTERIZATION

We calculated our motor's K_b , K_τ , and K_m using the following equations:

$$K_b = \frac{V_{amplitude}}{\omega}, \quad K_\tau = 3K_b, \quad K_m = \frac{K_\tau}{\sqrt{R_{coil}}}$$

where $V_{amplitude} = \frac{V_{peak-to-peak}}{2}$ and $\omega = \frac{4\pi f}{n_p}$.

For this motor $n_p = 8$. Note that the relationship between K_τ and K_b shown above is only true for three-phase permanent magnet motors.

From the back EMF waveforms in Fig. 6, we see that $V_{peak-to-peak} = 157.50$ mV, meaning that $V_{amplitude} = 78.75$ mV. We also see that the frequency of the corresponding period is 26.667 Hz. Using the formulas above, we calculate that:

$$K_b = 0.00188[Vs] \approx 0.002[Vs]$$

$$K_\tau = 3 * 0.00188[\frac{Nm}{A}] \approx 0.006[\frac{Nm}{A}]$$

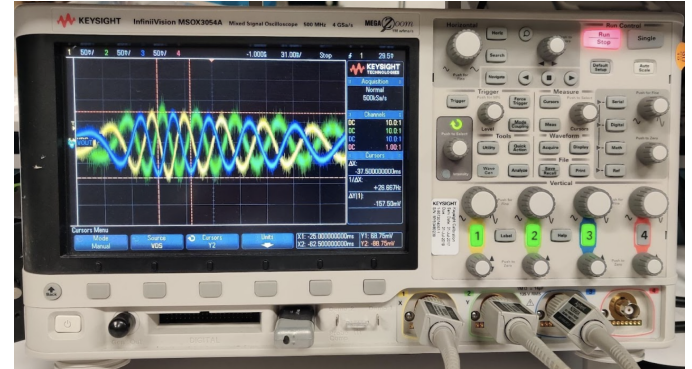


Fig. 6. Oscilloscope reading of Back EMF waveforms from manually spinning the motor. The three phases are 120° out of phase as expected. The two vertical cursors measure the period of a single phase, and the two horizontal cursors measure the corresponding peak-to-peak voltage.

Since motors are usually rated by their K_v , we also calculated the K_v of the motor. Using the equation

$$K_v = \frac{1}{K_b}$$

along with the K_b calculated above, we calculated that:

$$K_v = \frac{1}{K_b} = \frac{1}{0.00188} = 531.915[\frac{1}{Vs}] = 5080[\frac{RPM}{V}]$$

We then measured the line to neutral resistance for each of the three phases and found that $R_{A,GND} = 0.452\Omega$, $R_{B,GND} = 0.460\Omega$, and $R_{C,GND} = 0.450\Omega$. We then approximated $R_{coil} = 0.454\Omega$, the average of the three line to neutral resistances. Using the coil resistance, we calculated that:

$$K_m = 0.0089[\frac{Nm}{\sqrt{W}}]$$

VII. LIFT GENERATED AS FUNCTION OF RPM

To characterize the lift of the motor, we placed the motor and its housing on a scale as shown in Fig. 7. We then zeroed the scale and drove the motor using the ESC. We drove the motor in such a way that the propeller pushed the air upwards and therefore pushed the motor into the scale. This generated a measurable weight that we converted into thrust using the following equation:

$$\text{Thrust} = \text{Weight} * g$$

where $g = 9.8 \text{ m/s}^2$.

This thrust calculation would be the equal to the lift generated by the motor if the motor were spun in the opposite direction, but that could have potentially posed a safety hazard in the lab.

To calculate RPM from the oscilloscope image in Fig. 8, the cursors were set across 4 cycles (8 peaks to denote 8 pole pairs), which is the time period for a single revolution of the rotor. We then calculated the RPM using the following equation:

$$\text{RPM} = \frac{60}{\Delta t}$$



Fig. 7. Setup of motor and housing sitting on a scale which was used to measure the thrust generated by the motor as various RPMs.

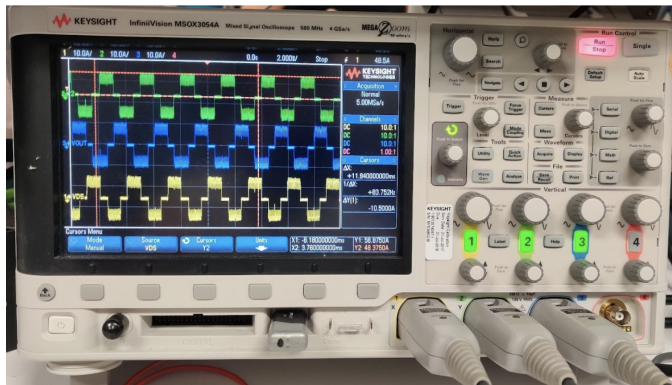
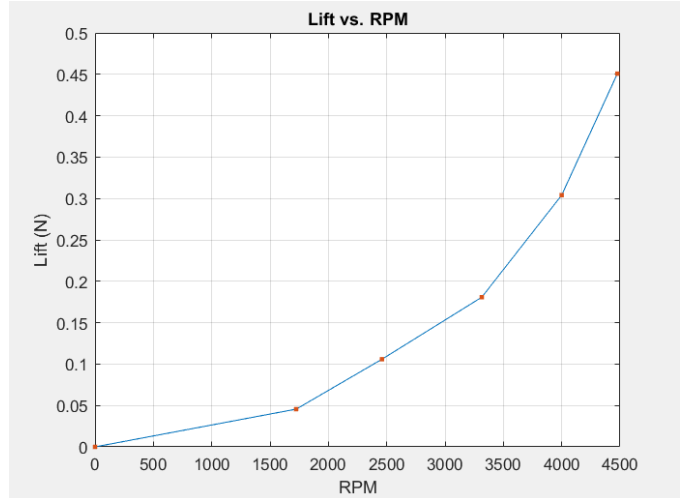


Fig. 8. Oscilloscope reading of current waveforms from driving the motor with the ESC and servo tester. The three phases are 120° out of phase as expected. The two vertical cursors measure 4 cycles of a single phase, and the two horizontal cursors measure the corresponding current amplitude.

We calculated the lift generated by our motor and propeller system at five different RPMs shown in Fig. 9. We see that the lift generated scales quadratically with RPM. The maximum speed measured in our testing was 5025 RPM (at 10V input), but we were unable to get a reliable lift measurement at this speed as the motor housing was quickly moving around on the surface of the scale. The current waveforms in Fig. 8 are from the 5025 RPM test.

VIII. CONCLUSION

To conclude, the design, fabrication, characterization, and lift testing of our 3D printed axial flux 3-phase permanent magnet motor in this project was a success. We demonstrate that 3D printing is a viable manufacturing method for prototype drone motors capable of spinning up to 5000 RPM. We characterized the motor by calculating the motor constants and the lift generated by the motor and propeller system as a function of RPM. However, the setup demonstrated in this paper could be improved by controlling the motor with a more advanced motor driver (i.e. ODrive v3.6 or other) to not require kickstarting the motor to get it to spin. Additionally, the lift testing apparatus could be improved by using more



Lift (N)	RPM
0	0
0.0447336	1724
0.105948	2459
0.1809945	3315
0.307053	4000
0.45126	4477

Fig. 9. Plot and table of motor and propeller system's generated lift as a function of RPM.

robust force sensors and holding the motor housing in place to prevent it from moving around during testing.

IX. ACKNOWLEDGEMENTS

We would like to thank Steve Clark, Jason Poon, and Aaron Goldin for their guidance and mentorship throughout the duration of this project.

REFERENCES

- [1] M.Bonnet, et al. “3D Magnetic Field Model of a Permanent Magnet Ironless Axial Flux Motor with Additively Manufactured Non-Active Parts” *19th edition of International Symposium on Electromagnetic Fields in Mechatronics, Electrical and Electronic Engineering (ISEF 2019)*, Aug 2019, Nancy, France.
- [2] M.Bonnet, et al. “Model of an Ironless Axial Flux Permanent Magnet Motor Based on the Field Produced by a Single Magnet” *IEEE Transactions on Magnetics, Institute of Electrical and Electronics Engineers*, 021, 57 (7), pp.1-4, Dec 2021.
- [3] C. Chan, “Axial-Field Electrical Machines - Design and Applications,” in *IEEE Transactions on Energy Conversion*, vol. EC-2, no. 2, pp. 294-300, June 1987, doi: 10.1109/TEC.1987.4765844.
- [4] Wu, D., Yang, J., Chan, T.F., Lai, C.S., Li, X., Yan, B., Lai, L.L., Wang, D., Gao, X. and Meng, K. (2019), Axial-flux permanent-magnet synchronous generator with coreless armature and non-integral coil-pole ratio. *IET Renewable Power Generation*, 13: 245-252. <https://doi.org/10.1049/iet-rpg.2018.5311>.